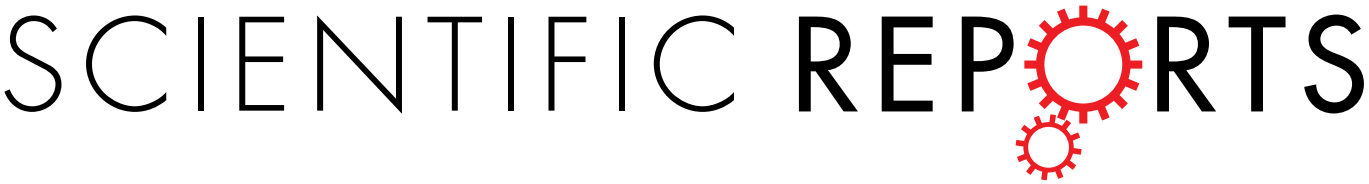

OPEN

# Excitonic structure and pumping power dependent emission blue-shift of type-II quantum dots

Received: 08 December 2016
Accepted: 27 February 2017
Published: 30 March 2017

Petr Klenovský[1,2], Petr Steindl[1,2] & Dominique Geffroy[2]

**In this work we study theoretically and experimentally the multi-particle structure of the so-called type-II quantum dots with spatially separated electrons and holes. Our calculations based on customarily developed full configuration interaction ap- proach reveal that exciton complexes containing holes interacting with two or more electrons exhibit fairly large antibinding energies. This effect is found to be the hallmark of the type-II confinement. In addition, an approximate self-consistent solution of the multi-exciton problem allows us to explain two pronounced phenomena: the blue-shift of the emission with pumping and the large inhomogeneous spectral broadening, both of those eluding explanation so far. The results are confirmed by detailed intensity and polarization resolved photoluminescence measurements on a number of type-II samples.**

Semiconductor quantum dots (QDs) are currently one of the most promising candidate systems for the realization of quantum cryptography protocols[1,2] or quantum gates[3,4] in the information technologies. However, so-far most of the research has been focused on so-called type-I QDs where both electrons and holes are confined inside the dot body. Notably, much theoretical and experimental work has been aimed at zeroing the fine-structure splitting (FSS) of the excitonic doublet by various methods[5–7]. On the other hand, research on type-II QDs[8–11] where electron and hole states are spatially separated has not experienced that much interest. This is particularly due to the smaller overlap of the quasiparticle wavefunctions leading to considerably reduced emission intensity and rate[12–15]. Moreover, the emission from type-II QDs is considerably and inhomogeneously broadened[16,17] compared to type I, and a large blue-shift of the emission energy with increasing laser pumping has been observed[18,19]. Apart from a rich physics, the spatial separation of the carriers in systems with type-II confinement provides several advantages compared to type I. In particular, a naturally small FSS was predicted to occur, see ref. 20, as well as molecular-like states[12,13,21] that might be used for the design of quantum gates, see ref. 22. As a result, type-II QDs can be used in quantum information technology without the need for elaborate post-processing of the quantum states.

Although we have recently demonstrated a method to determine the vertical position of the hole wavefunction in real samples[23], more obstacles associated with type-II QDs remain. In particular, because of the inhomogeneous broadening of the spectral bands there has been only a small amount of experimental[24] or theoretical[25,26] studies of the excitonic structure of type-II QDs. Furthermore, there is still an ongoing discussion about the physical nature of the emission energy blue-shift with pumping[27–30].

In this paper we address the aforementioned issues. We provide the theoretical description of the (multi-) excitonic structure of type-II QDs using a Full Configuration Interaction (CI) method developed for this purpose, as well as the experimental observation of the recombination of multi-particle states by intensity and polarization resolved photoluminescence (PL) measurements. Finally, we present a model, based on approximate self-consistent CI, of the pumping dependent energy blue-shift of the individual excitonic transitions seen in our PL experiments, and provide its physical interpretation.

Although our results are general, we have chosen GaAsSb capped InAs QDs in GaAs matrix as the test system. It is favored because this system allows for continuous change of the type of confinement by varying the Sb content in the GaAsSb capping layer (CL)[12].

[1]Central European Institute of Technology, Masaryk University, Kamenice 753/5, 62500 Brno, Czech Republic. [2]Department of Condensed Matter Physics, Faculty of Science, Masaryk University, Kotlářská 2, 61137 Brno, Czech Republic. Correspondence and requests for materials should be addressed to P.K. (email: klenovsky@physics.muni.cz)

## Theory

We have studied excited states involving several interacting quasi-particles using the full configuration interaction technique[31–34]. In this framework, the stationary Schrödinger equation to be solved reads

$$\hat{H}^M|M\rangle = M|M\rangle,\ M \equiv X^0,\ X^+,\ X^-,\ XX^0\ldots, \tag{1}$$

where $M$ is the eigenenergy of the (multi-)excitonic state $|M\rangle$ corresponding to $N_a$ and $N_b$ i.e. the numbers of particles $a$ and $b$, respectively, where $a, b \in \{e, h\}$ with $e$ standing for electron and $h$ for hole. The complexes investigated in this work are the neutral exciton $X^0$ ($N_e = 1, N_h = 1$), the positive trion $X^+$ ($N_e = 1, N_h = 2$), the negative trion $X^-$ ($N_e = 2, N_h = 1$), and the neutral biexciton $XX^0$ ($N_e = 2, N_h = 2$). We look for solutions of Eq. (1) in the form

$$|M\rangle > = \sum_m \eta_m |D_m^M\rangle \tag{2}$$

where $m$ runs over all configurations corresponding to the given $M$. $|D_m^M\rangle$ is the corresponding Slater determinant, which involves the single-particle states $\{\psi_i\}$, $i \in S_n$ (so that the cardinal of $S_n$ verifies **card** $(S_n) = N_a + N_b$). We solve variationally for the coefficients $\eta_m$, i.e. we solve the system of equations $\sum_m \langle D_n^M|\hat{H}^M|D_m^M\rangle \eta_m = M\eta_n$, under the normalization constraint $\sum_n |\eta_n|^2 = 1$.

The matrix elements of the Hamiltonian $\hat{H}^M$ in the basis of the Slater determinants are given by (see the Supplementary Section SI online for details of the derivation, and for the expression of the Coulomb matrix element $V_{ij,kl}$)

$$\begin{aligned}
\hat{H}^M_{nm} &\equiv \langle D_n^M|\hat{H}^M|D_m^M\rangle \\
&= \begin{cases}
\mathcal{E}_n^{(e)} - \mathcal{E}_n^{(h)} + \dfrac{1}{2}\displaystyle\sum_{i,j\in S_n} (V_{ij,ij} - V_{ij,ji}) & \text{if } n = m \\
\dfrac{1}{2}\displaystyle\sum_{j\in S_n} V_{ij,kj} - V_{ij,jk} & \text{if } D_n^M \text{ and } D_m^M \text{ differ by one single-particle state: } |D_n^M\rangle \\
& \quad \propto c_i^\dagger c_k |D_m^M\rangle \\
\dfrac{1}{2}(V_{ij,kl} - V_{ij,lk}) & \text{if } D_m^M \text{and } D_n^M \text{ differ by two single-particle states: } |D_n^M\rangle \\
& \quad \propto c_i^\dagger c_j^\dagger c_k c_l |D_m^M\rangle,\ k \\
& \quad < l,
\end{cases}
\end{aligned} \tag{3}$$

where $\mathcal{E}_n^{(e)}$ ($\mathcal{E}_n^{(h)}$) is the sum of the energies of the occupied single-particle electron (hole) states in the determinant $D_n^M$.

The oscillator strength of the interband optical transition $F_{fi}^M$ between the $i$-th and $f$-th eigenstate of the excitonic complex $M$, respectively, is found using Fermi's golden rule[34]

$$F_{fi}^M = \left|\left\langle M_f\middle|\hat{P}|M_i\right\rangle\right|^2, \tag{4}$$

where $|M_f\rangle$ is the final state after recombination of one electron-hole pair in $|M_i\rangle$. The operator $\hat{P}$ is defined by

$$\hat{P} = \sum_{rp} \langle \psi_{e_r}|\mathbf{e}\cdot\hat{\mathbf{p}}|\psi_{h_p}\rangle. \tag{5}$$

Here $\psi_e$ and $\psi_h$ are the single-particle wavefunctions for electrons and holes, respectively, $\mathbf{e}$ is the polarization vector, and $\hat{\mathbf{p}}$ the momentum operator. For more information of the implementation of CI used in our calculations, see the Supplementary Section SI.

## Results

**Excitonic structure of type-II QDs.** We have calculated the (multi-)excitonic structure of InAs/GaAsSb/GaAs QDs by the CI method, outlined in the previous section, coded in the Python 2.7 programming language[35]. The single-particle basis states were obtained from the Nextnano++ simulation package[36] that employs the envelope function approximation based on the eight-band $\mathbf{k}\cdot\mathbf{p}$ method. The simulated structure was a lens-shaped InAs QD with height of 4 nm and basis diameter of 16 nm. The In distribution in the QDs was either constant at 0.6, or trumpet-like[37,38]. The thickness $d$ and the Sb composition of the CL were varied during the calculations. For a side view of the structure, see panels (e) and (f) of Fig. 1. The physical properties of the simulated QDs were chosen so that the energy of $X^0$ approximately matches our experimental data, discussed in the next section.

In Fig. 1 (a) and (b)we show the calculated Sb content dependencies of the energy difference of $X^+$, $X^-$, and $XX^0$ from $X^0$. It can be clearly seen that the transition from type-I to type-II confinement is associated with $XX^0$ and $X^-$ becoming significantly anti-binding while $X^+$ remains binding for all Sb contents. Depending on the shape and on the In composition profile of the type-II QD, $XX^0 - 2X^0$ varies from 80 meV for a lens-shaped QD with spatially constant In content[13,23], up to 200 meV for a pyramidal QD with trumpet In profile[12].

These trends can be understood based on the fact that for type-II structures holes are located in CL whereas electrons in QD body, see the inset of Fig. 1(b) for the hole, and panels (e) and (f) for the electron

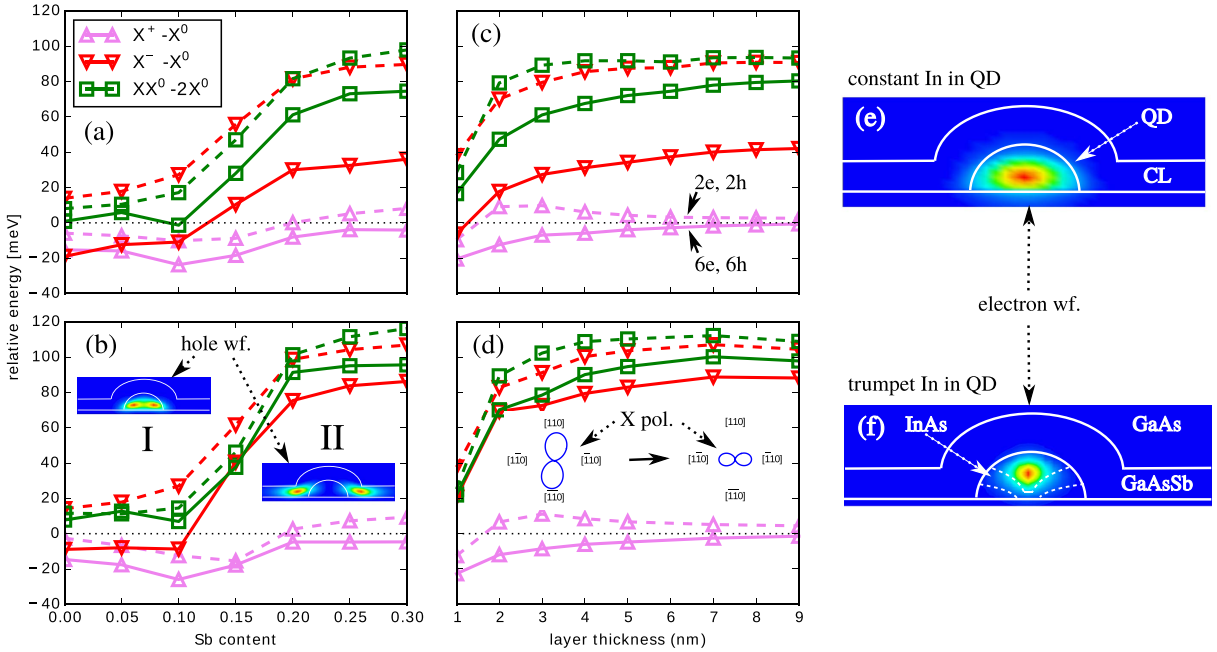


**Figure 1.** (**a**,**b**) Energies of the complexes $X^+$, $X^-$, and $XX^0$ with respect to that of $X^0$ as functions of Sb content for constant [trumpet] In composition in QD, and $d = 5$ nm. Panel (c,d) shows the same quantities as functions of $d$ for a fixed Sb content of 0.24. The points connected with broken curves correspond to calculations with 2 electron and 2 hole single-particle basis states while those connected by the full curves represent the results obtained for 6 by 6 basis. The labels I and II in (**b**) represent the type of confinement and the insets the corresponding $(1\bar{1}0)$ plane cuts of the hole probability densities. The inset of (**d**) shows the polarization of the emission of $X$ for thin and thick capping layers. Panels (e) and (f) show the simulated structures and the probability density of the electron wavefunction in QD for constant and trumpet In distribution, respectively.

wavefunctions[12]. Because of that, the electron-hole attractive Coulomb interaction $J_{eh}$ is significantly reduced while the electron-electron $J_{ee}$ and hole-hole $J_{hh}$ repulsive potentials are either not changed at all or reduced much less. Since $XX^0 - 2X^0 \approx J_{ee} + J_{hh} - 2J_{eh}$ and $X^- - X^0 \approx J_{ee} - J_{eh}$, and considering that the wavefunctions of electrons do not change much with the Sb content[12], one concludes that the dependencies are mainly governed by the reduction of $J_{eh}$, and one indeed expects that those should share a similar energy increase. On the other hand, changes in $X^+ - X^0 \approx J_{hh} - J_{eh}$ should be much smaller since the hole wavefunction tends to be segmented for type-II confinement and becomes more spatially spread in CL. This implies that $J_{hh}$ is reduced alongside with $J_{eh}$ for larger Sb.

We can characterize the impact of correlation in the quantum dot by evaluating the quantity $E_{\mathrm{corr}}$, defined as the difference between the energy of a complex (e.g. $X^+$), calculated using a small number of single-particle states (2 electron and 2 hole single-particle states), and the energy of the same complex, calculated using a large number of single-particle states (the maximum is 6 electron and 6 hole single-particle basis states in the present study). While the magnitude of $E_{\mathrm{corr}}$ on the studied complexes for QDs with trumpet In composition is generally not very large [see Fig. 1(b) and (d)] it can increase up to $-50$ meV for QDs with constant In content [see Fig. 1(a)]. In all cases, $E_{\mathrm{corr}}$ tends to scale as $E_{\mathrm{corr}}(X^+) < E_{\mathrm{corr}}(XX^0) < E_{\mathrm{corr}}(X^-)$ in type-II QDs. The difference in the magnitude of $E_{\mathrm{corr}}$ on the $X^-$ and $X^+$ complexes is consistent with the different spatial spread of the single-particle electron and hole wavefunctions, respectively, which is smaller for the former. Similarly, QDs with a constant In composition behave as wider effective quantum wells for electrons, compared with their trumpet-like counterparts. This allows for an energetically more favorable spatial distribution of the single-particle wavefunctions and, thus, a larger reduction of $J_{ee}$ by $E_{\mathrm{corr}}$. Schliwa and coworkers observed similar trends for InGaAs/GaAs type-I QDs[32].

The results of $XX^0 - 2X^0$, $X^- - X^0$, and $X^+ - X^0$ as functions of $d$ for a fixed Sb content of 0.24 can be found in panels (c) and (d) of Fig. 1; the content was chosen so that the system generally corresponds to type-II confinement. However, for thin layers the energy of holes is too large for localization of the hole ground state in the CL and the system is type I[12], accompanied by a small value of $XX^0 - 2X^0$. However, further increase of $d$ brings the system to type-II confinement, marked again by enormously anti-binding $XX^0$ and $X^-$. It can be concluded that a strongly anti-binding biexciton is a hallmark of the type-II systems.

Moreover, the increase of $d$ induces a change in the vertical position of the hole wavefunction from the base of the QD to a location above its apex. This is connected with a change in the orientation of the emission polarization, and allows for the determination of the vertical position of the hole from polarization resolved PL measurements, see ref. 23. This effect is preserved also for states calculated by CI, see inset of Figs 1(d) and 2. However, one needs to calculate the emission of $X$ as $\sum_k F_k^X$ where $k$ runs over two bright excitonic eigenstates lowest in energy. The method is explained in panels (a) and (b) of Fig. 2. In (a) we show the polar graph of $F^X$ for the two lowest states of $X^0$, along different crystallographic directions. These are polarized linearly due to the structural anisotropy of the

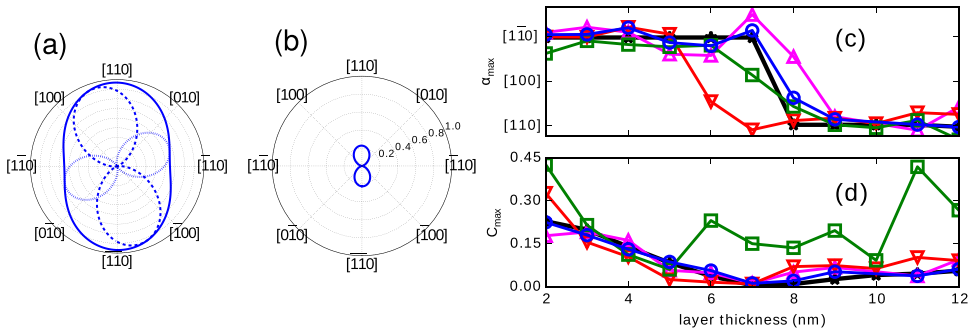


**Figure 2.** (**a**) Polar graph of $F^X$ for two bright states lowest in energy (broken and dotted curve) and that for $\sum_{k=1}^{2} {F_k}^X$ (full curve). Panel (b) shows the polar graph of the degree of polarization $C(\alpha)$ for $\sum_{i=1}^{4} {F_i}^X$ (see text). Polarization azimuth $\alpha_{max}$ and the maximum degree of polarization $C_{max}$ as functions of CL thickness $d$ are given in panels (c) and (d), respectively. The data are plotted for $X$ (blue rings), $X^+$ (magenta upward triangles), $X^-$ (red downward triangles), and $XX$ (green squares). The multi-particle states were obtained using CI with 6 single-particle electron and 6 hole wavefunctions. For comparison we include the data taken from ref. 23 (black stars).

QDs and perpendicularly to each other, being oriented either close to [110] or [1$\bar{1}$0]. The excitonic state with larger $F^X$ is oriented along the former direction and so is the polarization anisotropy of $\sum_{k=1}^{2} = {F_k}^X$ for the exemplar QD. We characterize this, similarly to ref. 23, by a degree of polarization $C$ defined by

$$C(\alpha) = \frac{F(\alpha) - F_{\min}}{F_{\max} + F_{\min}}, \tag{6}$$

where $\alpha$ is the angle corresponding to the crystallographic direction in the plane of the sample; $F_{max}$ and $F_{min}$ are the maximum and minimum oscillator strengths, respectively. The maximum degree of polarization $C_{max}$ occurs in direction given by an angle $\alpha_{max}$. We note that the reason for monitoring the polarization anisotropy of $\sum_{k=1}^{2} {F_k}^X$ instead of that of $F^X$ is due to the fact that we study ensemble PL in this work.

In panels (c) and (d) of Fig. 2 we give $C_{max}$ and $\alpha_{max}$, respectively, for $X^0$, $X^+$, $X^-$, and $XX^0$ as functions of $d$. It can be clearly seen that the polarization properties of the sum of multi-particle states mostly mimic that for $X^0$. This of course reflects the fact that on performing $\sum_k F_k^M$ the fine-structure of excitonic complexes is lost. We use this property to determine the origin of the multi-excitonic complexes in our PL measurements presented in the next section.

## Experiment

Four samples of InAs QDs with GaAsSb CL and a sample of InGaAs/GaAs QDs, were fabricated by the low pressure metal-organic vapor phase epitaxy (MOVPE)[39]. Detailed information about the sample preparation might be found in ref. 23. We note here only that in order to obtain statistically significant variability of QDs differing in sizes, shapes, CL thicknesses and compositions, the growth was performed on a non-rotating susceptor.

The PL measurements were performed using a NT-MDT Ntegra-Spectra spectrometer. The samples were positioned in the cryostat, cooled to liquid nitrogen temperature (LN2) and pumped by a solid-state laser with a wavelength of 785 nm. The maximum laser power on the sample surface was 5 mW on the 150 $\mu$m$^2$ area, and was varied by a tunable neutral density (ND) filter. The polarization of the PL was analyzed by a rotating achromatic half-wave plate followed by a fixed linear polarizer. The PL signal was dispersed by a 150 grooves/mm ruled grating and detected by the InGaAs line-CCD camera, cooled to minus 90. In every experiment, PL light was collected from a large number of QDs ($\sim$3000).

We show our experimental results for one sample with type-II QDs in Fig. 3. We have measured PL spectra for a set of values of the laser pumping power $P$. For each of these values also the polarization anisotropy $C(\alpha)$ defined by Eq. (6) was obtained. The spectra were fitted by a sum of Gaussian functions and to each of those an appropriate recombination channel was assigned, see Fig. 3(a). The assignment was based on (i) the exponent $a$ of $F \propto P^a$, see Fig. 3(b), (ii) the azimuth $\alpha_{max}$, see the polar graphs at the bottom of Fig. 3, and (iii) comparison with theoretical predictions. The type of confinement was determined, as it is usually done[16,40], by observation of the blue-shift of the normalized PL spectra with $P$ (or its absence), see panel (a).

We have clearly identified the recombination of $X^0$, $X^-$, and $XX^0$ in our spectra. The measured energy separations of the latter two from $X^0$ are $X^- - X^0 = 76$ meV and $XX^0 - 2X^0 = 162$ meV, i.e. considerably shifted to higher energies as predicted by our theory, see Fig. 1. As expected, the band $X^+$ cannot be distinguished from $X^0$ in our PL measurements since $X^+ - X^0$ is much smaller than the inhomogeneous spectral broadening of the emission bands from GaAsSb capped InAs QDs.

The band with the largest energy $E$ [shaded part in Fig. 3(a)] is attributed to the recombination between electrons confined due to strain at the interface between bulk GaAs, and holes within the GaAsSb CL, see also inset of Fig. 3. This transition is purely of type-II nature and exhibits a very large blue-shift with increasing $P$. A similar recombination pattern has been observed previously for InAsSb QDs[41] and is also responsible for the no-phonon emission from SiGe/Si QDs[42].

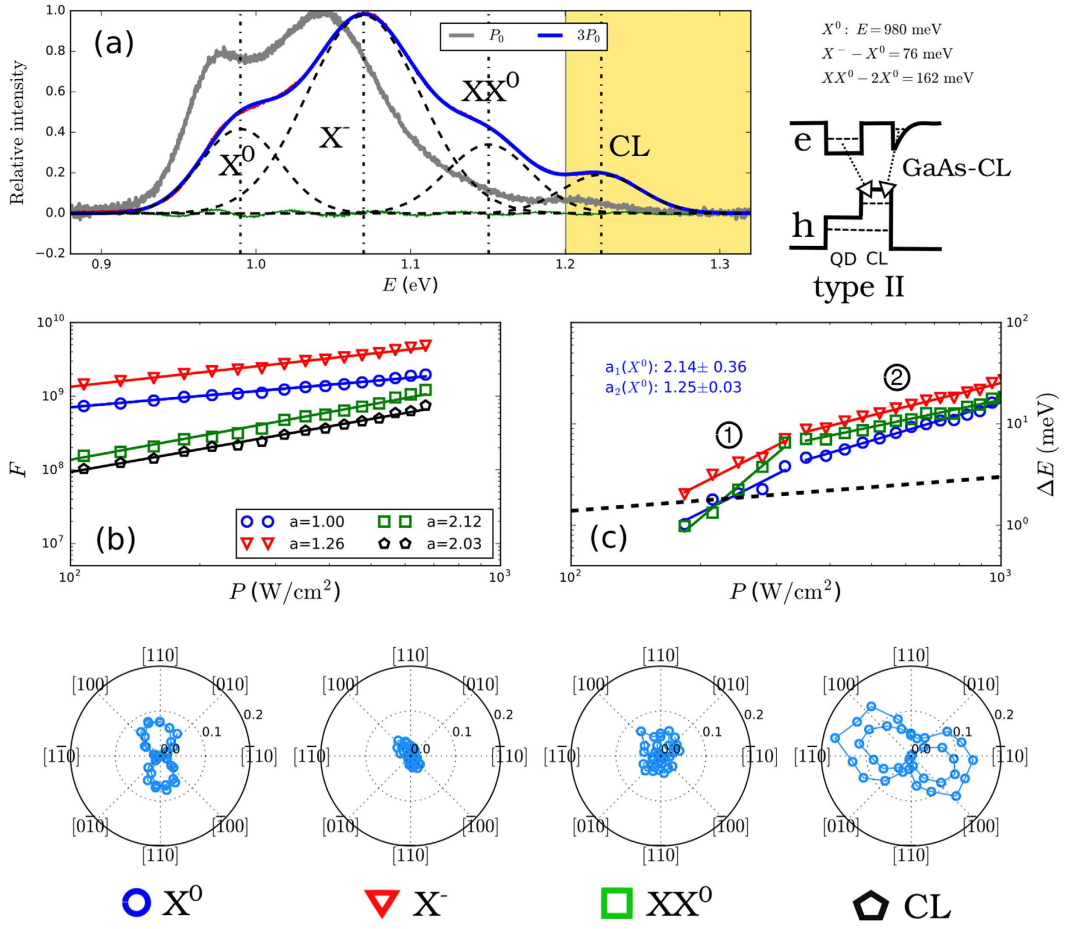


**Figure 3.** (**a**) PL spectra of GaAsSb capped InAs type-II QDs measured for two pumping powers $P$ (grey and blue curves). The fit by the sum of Gaussian curves is shown for $3P_0$ (blue curve) and the individual bands corresponding to different multi-excitonic transitions are shown by broken curves. The difference between data and fit is represented by green curve. The dotted vertical lines indicate the energies of the bands for $3P_0$. The yellow shaded part of the graph corresponds to the recombination between bulk GaAs and CL. The inset next to panel (a) gives the spectral positions of of the three bands and a schematic band diagram of the recombination processes (not in scale). In (**b**) we show the $P$-dependence of the oscillator strength $F$ of the identified bands in log-log scale and their fits by linear lines, respectively, for $X^0$ (blue circles), $X^-$ (red triangles), $XX^0$ (green squares), and that for the transition between bulk GaAs and CL (black pentagons). The slopes $a$ (i.e. exponents in the linear plots) of the fitted lines are given in the inset of panel (b), for clarity they were normalized so that $a = 1$ for $X^0$. Panel (c) depicts the change of the emission energy $\Delta E$ with $P$ in log-log scale. Except of GaAs-CL transition which was omitted, the labels are the same as in (**b**) and the data were fitted by two linear functions in segments 1 and 2 (see text). The fitted slopes (i.e. exponents of the dependencies) $a_1$ and $a_2$ for $X^0$ are given in the inset. The $\Delta E \sim P^{1/3}$ dependence of ref. 29 is shown by broke curve. The polar graphs at the bottom show $C(\alpha)$ of individual identified bands.

In Fig. 3(c) we show in log-log scale the energy shift of the PL bands (excluding GaAs-CL transition) with increasing $P$, i.e. $\Delta E(P) = E^M(P) - E^M(P_{min})$ where $P_{min}$ is the lowest value of $P$ used in our measurements. In addition to a considerable blue-shift of the bands, which is as large as 30 meV for our values of $P$, it can be seen that (i) $\Delta E$ is different for different $M$ and (ii) there is an edge in the power dependencies meaning that $\Delta E(P)$ does not follow the simple form of $\Delta E \sim P^a$ for all values of $P$ but that for each of the two segments 1 and 2 a different exponent $a_1 = 2.14 \pm 0.36$ and $a_2 = 1.25 \pm 0.03$ seem more appropriate. That effect, observed also elsewhere[43], is significantly different from the $\Delta E \sim P^{1/3}$ dependency predicted in ref. 29, which is displayed as a broken curve for comparison. Moreover, there are differences between the values of the exponents for different complexes. We postpone the explanation of the pumping dependent blue-shift to the next section.

The polar graphs at the bottom of Fig. 3 show that the radiation due to the recombination of $M$s from the dots is polarized along [110] crystallographic direction. The fact that all $M$s share the same $\alpha_{max}$ confirms our prediction shown in Fig. 2. The polarization along the [110] in turn means that the holes are located in the CL close to the QD base[23] for this particular sample. Moreover, the measurements of $\alpha_{max}$ allow us to clearly distinguish the GaAs-CL band from the recombinations originating from QD states owing to their perpendicular polarization. A similar method of assignment was used in earlier studies, see e.g. ref. 44.

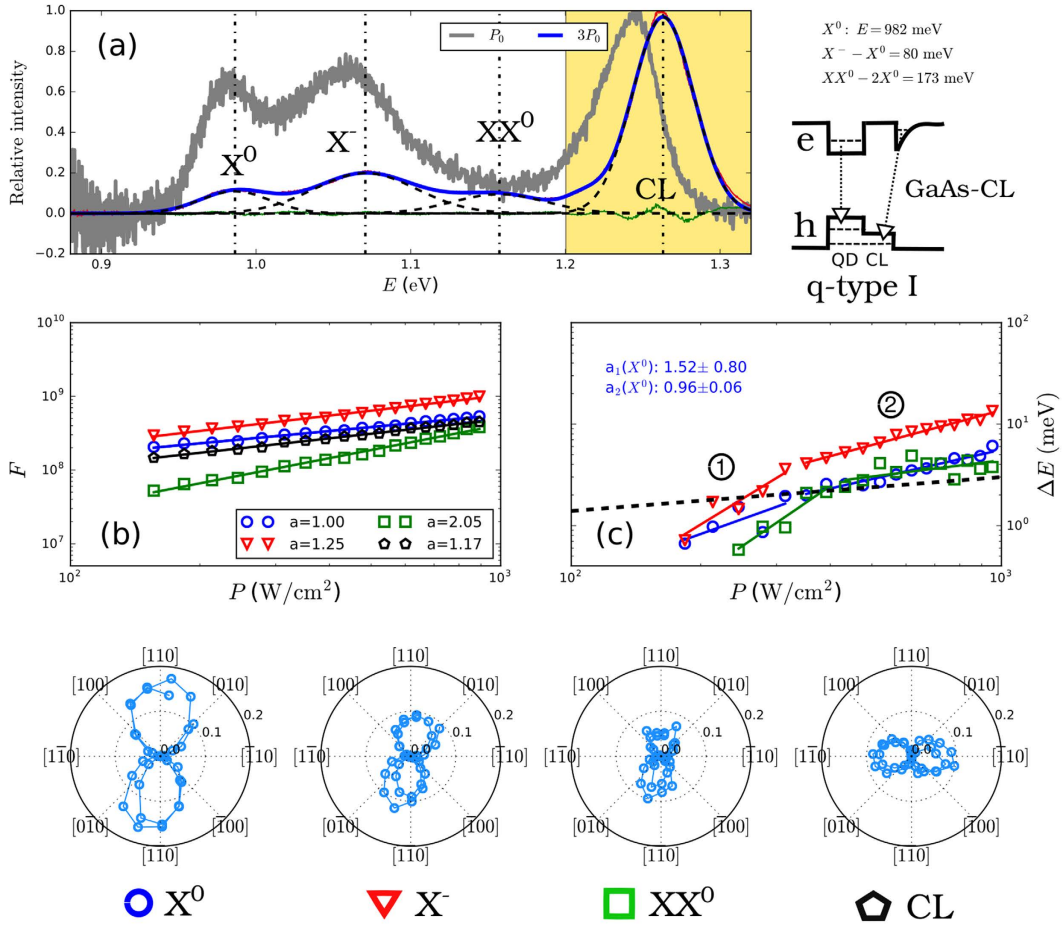


**Figure 4. PL spectra of GaAsSb capped InAs q-type-I QDs.** The results are given in the same nomenclature as in Fig. 3.

In Fig. 4 we show PL measurements of QDs with type-I confinement in very much the same way as in Fig. 3. We again identify $X^0$, $X^-$, $XX^0$ and the GaAs-CL transition, respectively. Interestingly, the relative positions of $M$s are similar to type-II QDs, with $X^- - X^0 = 80$ meV and $XX^0 - 2X^0 = 173$ meV. This is due to the fact that even a rather small increase in CL thickness results in a considerable increase of $X^- - X^0$ and $XX^0 - 2X^0$, respectively, see Fig. 1. In fact, the type of confinement is not purely of type-I in GaAsSb capped InAs QDs for Sb contents different from zero, since even a slight increase of that lowers the confinement for holes in the CL with respect to GaAs[12], see inset of Fig. 4. Thus, the excited single-particle states tend to be partly localized in the CL, which results in a slight blue-shift of $X^0$ with increasing $P$ and also $a_1 = 1.52 \pm 0.80$ and $a_2 = 0.96 \pm 0.06$ are not equal to zero, respectively, see Fig. 4(c). We call this type of confinement "quasi-type-I" (q-type-I). For results of the true type-I confinement represented by InAs/GaAs QDs for which no blue-shift of $X^0$ with $P$ is observed and $a \approx 0$ see Supplementary Fig. S1. We note that slightly larger values of $X^- - X^0$ and $XX^0 - 2X^0$ for type-II and q-type-I in Figs 3 and 4, respectively, compared to Fig. 1 are probably due to the spatial inhomogeneity of the In distribution in the QDs, and of Sb in the CL, which were not considered in our theory.

The polarization anisotropy of q-type-I QDs is again along [110], see bottom of Fig. 4, and is larger than for type II in agreement with our theoretical predictions in Fig. 2(d) for very thin CL. Again the GaAs-CL band is identified by its perpendicular polarization compared to the emission from QD bands. Note that the energy difference of that band from $X^0$ is larger compared with the type II. This is consistent with our interpretation, Cf. insets of Figs 3 and 4. Since the confinement for holes in the CL is larger for type I than for type II, the emission energy of GaAs-CL band is larger in type I. The energy of the GaAs-CL band also blue-shifts with pumping by a much larger amount than for the q-type-I QD bands and, thus, this structure represents a coexistence of type-I and type-II confinement[45].

In order to make our results more general we repeated the aforementioned measurements on 16 different QD samples. The results of those are given in the Supplementary Fig. S2 for the exponent in $F = bP^a$, S3 for the mean emission energy shift, S4 for the mean $a$ in $\Delta E = bP^a$, and S5 for $\alpha_{max}$, and $C_{max}$, respectively.

**Model of blue-shift.** We comment here on the origin of the blue-shift of the emission energy $\Delta E$ with increasing $P$ in type II which we observe in our PL measurements. Currently, two competing hypotheses are put forward in this respect: the "state-filling" model, stemming from the observation of the large radiative lifetime of the emission from type-II QDs[15,28,46–48] which occurs due to the smaller overlap between electron and hole

wavefunctions[12,14]. If the pumping rate exceeds the emission rate of the ground state transition, which is often the case in type-II QDs, a larger proportion of the radiative transitions between electronic levels higher in energy than the ground state results, leading to a blue-shift effect[27]. In addition to this energetic aspect, the spatial localization of the wave functions associated with the states involved in the state-filling induces a capacitive charging effect[43], also contributing to the overall blue-shift of the emission. Using a model in which those two contributions can be disentangled, it was recently claimed that the spatial contribution (capacitive charging) has a much larger contribution than the purely energetic effect[49]. While our modeling approach does not allow a comparison of the relative contribution of each effect, it does intrinsically include both effects, and treats them on an equal footing.

The second hypothesis is called "band-bending". It explains the blue-shift as a change of the confinement potential for holes close to the QD[16,18,29,30]. In the specific framework of infinite triangular quantum wells, it was speculated that this mechanism induces a $\Delta E \propto P^{1/3}$ dependence[30,50,51]. While the validity of this power law for different systems is arguable, it was often used in the literature for discussing the properties of GaSb/GaAs QDs[29,52]. We follow this usage and thus include a comparison to this power law in the discussion of our results. The fundamental difference between these two hypotheses lies in whether or not the energies of the quantized levels change with $P$ in type-II QDs. We now attempt to simulate the experimentally observed blue-shift, and judge its consistency with either hypothesis.

Our experimental results are presented in Figs 3 and 4. It can be seen that they are not consistent with the power law usually associated with band-bending, and require a specific interpretation. To this end, we follow an approach similar to that of Gradkowski *et al.*, see ref. 27. Since the electronic states in QDs are multi-particle in nature we proceed by employing a semi-self-consistent CI (SSCCI) approach to characterize the energy shift with $P$. In SSCCI we first define a certain concentration of background electron $c_e$ and hole $c_h$ charges, the former only in the QD body and the latter just in CL, respectively, reflecting the spatially indirect nature of charges in type-II system. The concentrations are defined in such a way that $c_h - c_e = 0$, corresponding to a steady-state pumping. In other parts of the simulated structure (GaAs matrix) we set $c_h = c_e = 0$, reflecting the fact that the recombination there is spatially direct. The presence of $c_e$ and $c_h$ results in a background electric potential in QD and CL, respectively. We solve self-consistently the single-particle Schrödinger and Poisson equations for the system in the presence of these potentials. The wavefunctions obtained in that way are then fed into our CI solver. We, however, set all diagonal matrix elements of $J_{eh}$ resulting from the CI calculation to zero since we assume those to be already included in the single-particle energies obtained from the preceding self-consistent cycle.

On the other hand, the correspondence with the experiment is obtained by ref. 51

$$P = \frac{10^6 \gamma E_l}{\alpha} c_q^2, \tag{7}$$

where $c_q = c_e = c_h$ is the number of electron-hole pairs generated by a laser light with the energy $E_l$ (in our case 1.58 eV), $\alpha$ is the absorption coefficient of the sample material ($2.0 \times 10^4\,\mathrm{cm}^{-1}$ for GaAs[53]), and $\gamma$ is the radiative recombination coefficient ($7.0 \times 10^{-10}\,\mathrm{cm}^3\,\mathrm{s}^{-1}$ in the case of GaAs[53]).

The results of the blue-shift of multi-excitonic energies with $P$ calculated by SSCCI are presented in Fig. 5 for CL thicknesses of 3 and 8 nm. Clearly, our model correctly predicts the "bending" of $\Delta E(P)$ in panels (c) of Figs 3 and 4, and the presence of different slopes in the log-log graph [indicated by marks 1 and 2 in Fig. 5(a)]. The fitted exponents (slopes in log-log graphs) are $a_1 = 0.87 \pm 0.02$ and $a_2 = 0.07 \pm 0.02$ for $d = 3$ nm, and $a_1 = 0.54 \pm 0.02$ for 8 nm, respectively. This matches the trends of Fig. 3 fairly well. For type II the exponent in sector 1 decreases while that in sector 2 increases with increasing $d$, up to an approximate $\Delta E \sim P^{1/3}$ dependence reached for thick CLs. The blue-shift is accompanied by a change of the spatial distribution of the hole wavefunction[27], see insets of Fig. 5(b): holes are "squeezed" towards the QD body and, thus, towards the electrons[27,54].

The difference between the $a_1$ exponents for thinner and thicker CLs, respectively, can be qualitatively understood by inspecting the change in the lateral electron-hole dipole moment $p_{eh,xy}$ with $P$. We focus on the lateral plane only, where the anisotropy of the confinement potential for holes due to piezoelectricity $V_{xy}^{\mathrm{piez}}$ is strongest[12]. The total lateral potential for holes in type-II QDs might be written as $V_{xy}^{\mathrm{total}} = V_{xy}^{\mathrm{bulk}} - V_{xy}^{\mathrm{piez}}$, where $V_{xy}^{\mathrm{bulk}}$ is the energy of the holes in bulk semiconductor. The spatial extent of the hole wavefunction is shifted towards that of the electrons, confined in QD body for type II, with increasing $P$. Thus, $V_{xy}^{\mathrm{piez}}$ is reduced, so that both $V_{xy}^{\mathrm{total}}$ and the single-particle transition energies increase. By noticing that $p_{eh,xy}$ is larger in the QDs with a thin CL than in those with a thick CL, we can infer that the rate of blue-shift of single-particle transition energies with $P$ should be larger for QDs with thinner CLs.

The mechanism just described can only be valid, however, up to some finite pumping power $P_{\mathrm{crit}}$: at some point, the drift of the hole towards the electrons is hampered by the confinement imposed by the QD body, lest the hole either collapses into QD and the system transfers to the type-I confinement, or it is not bound in the structure anymore. At this point, we should observe a reduction in the rate of the change of the dipole. Following this scenario, $P_{\mathrm{crit}}$ must be smaller for thinner CLs and should increase with $d$, see Supplementary Fig. S6 for $d = 5$ nm.

The meaning of $c_e$ and $c_h$ in our calculations is that of an average occupation of charge traps[55] in QD and CL, respectively, changing from less than one to two electron-hole pairs per QD volume as $P$ is increased. In our understanding, there is probably an important contribution of trap-state filling effect to the emission blue-shift with pumping in type-II. This is consistent with the inhomogeneously broadened spectra of single type-II QDs observed elsewhere[56,57], given the known link between trap filling and spectral broadening. We note that non-broadened recombination from type-II QDs might be experimentally measured, e.g. by using photon correlation Fourier spectroscopy[58,59]. Finally, our model of blue-shift of emission energy with $P$ is more consistent with the "band-bending" hypothesis presented above if the changes of the confinement potential of quasiparticles are due to filling of charge traps.

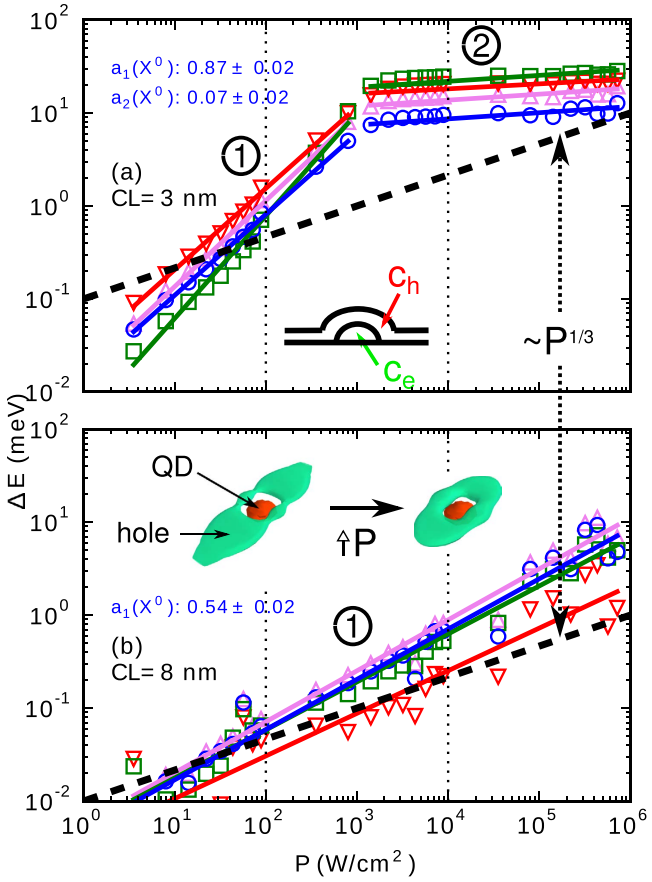


**Figure 5.** Energy shift $\Delta E$ versus $P$ for CL thicknesses $d$ of (**a**) 3 nm and (**b**) 8 nm. The results are shown for $X^0$ (blue circles), $X^+$ (magenta upward triangles), $X^-$ (red downward triangles), and $XX^0$ (green squares). The inset in (**a**) depicts th e background electron ($c_e$) concentration in QD and hole ($c_h$) in CL. The inset in (**b**) gives the the ground state hole probability densities for $d = 8$ nm and two values of $P$. The wavefunctions are given as green isosurfaces encircling 50% of the probability; the dot is marked as a red lens in the middle of the hole wavefunction. The parts of the wavefunction with largest probability density are oriented along the [110] direction. The numbers 1 and 2 mark different segments of the dependency similarly to Figs 3 and 4, respectively. The fitted values of the exponents $a_1$ and $a_2$ for $X^0$ are given in the insets of both panels. The dotted vertical lines in both panels roughly border the intervals where we have performed the measurements in Figs 3 and 4.

## Conclusions

We have studied the excitonic structure of type-II quantum dots both theoretically using the full configuration interaction method and experimentally by intensity and polarization resolved photoluminescence spectroscopy. We have found that the multi-particle complexes containing more electrons than holes in type II are typically considerably antibinding compared to type I, up to almost 200 meV for biexcitons. Furthermore, the polarization resolved photoluminescence measurements enabled us to discriminate spatially different recombination channels in our structures and revealed the coexistence of type-I and type-II confinement. Finally, the approximate self-consistent multi-particle calculations modeled our experimentally observed blue-shift of the emission with pumping in type II and provided an insight into the nature of that, being due to the filling of trap states, explaining also the reason for the large inhomogeneous spectral broadening of the emission bands of type-II QDs.

## References

1. Muller, M., Bounouar, S., Jons, K. D., Glassl, M. & Michler, P. On-demand generation of indistinguishable polarization-entangled photon pairs. *Nature Photonics* **8,** 224–228 (2014).
2. Strauf, S. *et al.* High-frequency single-photon source with polarization control. *Nature Photonics* **1,** 704–708 (2007).
3. Stevenson, R. M. *et al.* A semiconductor source of triggered entangled photon pairs. *Nature* **439,** 179–182 (2006).
4. Rodt, S., Schliwa, A., Potschke, K., Guffarth, F. & Bimberg, D. Correlation of structural and few-particle properties of self-organized inas/gaas quantum dots. *Phys. Rev. B* **71,** 155325 (2005).
5. Gerardot, B. D. *et al.* Manipulating exciton fine structure in quantum dots with a lateral electric field. *Appl. Phys. Lett.* **90,** 041101 (2007).
6. Plumhof, J. D. *et al.* Strain-induced anticrossing of bright exciton levels in single self-assembled gaas/alxga1-xas and inxga1-xas/gaas quantum dots. *Phys. Rev. B* **83,** 121302 (2011).
7. Trotta, R. *et al.* Nanomembrane quantum-light-emitting diodes integrated onto piezoelectric actuators. *Adv. Mat.* **24,** 2668 (2012).

8. Akahane, K., Yamamoto, N. & Ohtani, N. Long-wavelength light emission from inas quantum dots covered by gaassb grown on gaas substrates. *Physica E* **21,** 295 (2004).
9. Brunner, J. *et al.* Excitonic luminescence from locally grown sige wires and dots. *Appl. Phys. Lett.* **64,** 994–996 (1994).
10. Kim, S., Fisher, B., Eisler, H. J. & Bawendi, M. Type-ii quantum dots: Cdte/cdse(core/shell) and cdse/zinte(core/shell) heterostructures. *J. Am. Chem. Soc.* **125,** 11466–11467 (2003).
11. Stracke, G. *et al.* Indirect and direct optical transitions in in0.5ga0.5as/gap quantum dots. *Appl. Phys. Lett.* **104,** 123107 (2014).
12. Klenovský, P., Krápek, V., Munzar, D. & Humlícek, J. Electronic structure of inas quantum dots with gaassb strain reducing layer: Localization of holes and its effect on the optical properties. *Appl. Phys. Lett.* **97,** 203107 (2010).
13. Klenovský, P., Krápek, V., Munzar, D. & Humlícek, J. Modelling of electronic states in inas/gaas quantum dots with gaassb strain reducing overlayer. *J. Phys. Conf. Series* **245,** 012086 (2010).
14. Hsu, W.-T. *et al.* Effects of gaassb capping layer thickness on the optical properties of inas quantum dots. *Appl. Phys. Lett.* **99,** 073108 (2011).
15. Nishikawa, K. *et al.* Over 100 ns intrinsic radiative recombination lifetime in type ii inas/gaas1-xsbx quantum dots. *J. Appl. Phys.* **111,** 044325 (2012).
16. Liu, H. *et al.* Long-wavelength light emission and lasing from inas/gaas quantum dots covered by a gaassb strain-reducing layer. *Appl. Phys. Lett.* **86,** 143108 (2005).
17. Liu, H. *et al.* Room-temperature 1.6 mu m light emission from inas/gaas quantum dots with a thin gaassb cap layer. *J. Appl. Phys.* **99,** 046104 (2006).
18. Jin, C. Y. *et al.* Optical transitions in type-ii inas/gaas quantum dots covered by a gaassb strain-reducing layer. *Appl. Phys. Lett.* **91,** 021102 (2007).
19. Ulloa, J. M. *et al.* High efficient luminescence in type-ii gaassb-capped inas quantum dots upon annealing. *Appl. Phys. Lett.* **101,** 253112 (2012).
20. Krápek, V., Klenovský, P. & Šikola, T. Excitonic fine structure splitting in type-ii quantum dots. *Phys. Rev. B* **92,** 195430 (2015).
21. Krápek, V., Klenovský, P., Rastelli, A., Schmidt, O. G. & Munzar, D. Quantum entanglement in lateral gaas/algaas quantum dot molecules. *J. Phys. Conf. Series* **245,** 012027 (2010).
22. Klenovský, P., Krápek, V. & Humlícek, J. Type-ii inas/gaassb/gaas quantum dots as artificial quantum dot molecules. *Acta Physica Polonica A* **129** (2016).
23. Klenovský, P. *et al.* Polarization anisotropy of the emission from type-ii quantum dots. *Phys. Rev. B* **92,** 241302 (2015).
24. Matsuda, K. *et al.* Two-exciton state in gasb/gaas type ii quantum dots studied using near-field photoluminescence spectroscopy. *Appl. Phys. Lett.* **90,** 013101 (2007).
25. Rorison, J. M. A theory for excitons in type-ii quantum-dot systems. *Semicond. Sci. Technol.* **8,** 1470–1474 (1993).
26. Miloszewski, J. M., Tomic, S. & Binks, D. Theoretical studies of excitons in type ii cdse/cdte quantum dots. *4th Workshop On Theory, Modelling and Computational Methods For Semiconductors* (*tmcsiv*) **526** (2014).
27. Gradkowski, K. *et al.* Coulomb-induced emission dynamics and self-consistent calculations of type-ii sb-containing quantum dot systems. *Phys. Rev. B* **85,** 035432 (2012).
28. Young, M. P. *et al.* Photoluminescence studies of individual and few gasb/gaas quantum rings. *Aip Advances* **4,** 117127 (2014).
29. Hatami, F. *et al.* Carrier dynamics in type-ii gasb/gaas quantum dots. *Phys. Rev. B* **57,** 4635–4641 (1998).
30. Jo, M. *et al.* Origin of the blueshift of photoluminescence in a type-ii heterostructure. *Nanoscale Research Letters* **7,** 654 (2012).
31. Helgaker, T., Jorgensen, P. & Olsen, J. *Molecular Electronic-structure Theory* (Wiley, 2008).
32. Schliwa, A., Winkelnkemper, M. & Bimberg, D. Few-particle energies versus geometry and composition of inxga1-xas/gaas self-organized quantum dots. *Physical Review B* **79,** 075443 (2009).
33. Stier, O., Schliwa, A., Heitz, R., Grundmann, M. & Bimberg, D. Stability of biexcitons in pyramidal inas/gaas quantum dots. *Physica Status Solidi B-basic Research* **224,** 115–118 (2001).
34. Zielinski, M., Korkusinski, M. & Hawrylak, P. Atomistic tight-binding theory of multiexciton complexes in a self-assembled inas quantum dot. *Phys. Rev. B* **81,** 085301 (2010).
35. Python Software Foundation. Python Language Reference, version 2.7. Available at http://www.python.org.
36. Birner, S. *et al.* Nextnano: General purpose 3-d simulations. *IEEE Trans. El. Dev.* **54,** 2137 (2007).
37. Offermans, P. *et al.* Atomic-scale structure and photoluminescence of inas quantum dots in gaas and alas. *Phys. Rev. B* **72,** 165332 (2005).
38. Ulloa, J. M. *et al.* Suppression of inas/gaas quantum dot decomposition by the incorporation of a gaassb capping layer. *Appl. Phys. Lett.* **90,** 213105 (2007).
39. Hospodková, A. *et al.* Surface processes during growth of inas/gaas quantum dot structures monitored by reflectance anisotropy spectroscopy. *Surf. Sci.* **604,** 318–321 (2010).
40. Ulloa, J. M. *et al.* Analysis of the modified optical properties and band structure of gaas1-xsbx-capped inas/gaas quantum dots. *J. Appl. Phys.* **112,** 074311 (2012).
41. Mazur, Y. I. *et al.* Coexistence of type-i and type-ii band alignments in antimony-incorporated inassb quantum dot nanostructures. *Appl. Phys. Lett.* **100,** 033102 (2012).
42. Klenovský, P. *et al.* Excitation intensity dependence of photoluminescence spectra of sige quantum dots grown on prepatterned si substrates: Evidence for biexcitonic transition. *Phys. Rev. B* **86,** 115305 (2012).
43. Muller-Kirsch, L. *et al.* Many-particle effects in type ii quantum dots. *Applied Physics Letters* **78,** 1418–1420 (2001).
44. Alonso-Alvarez, D. *et al.* Strain balanced epitaxial stacks of quantum dots and quantum posts. *Advanced Materials* **23,** 5256–5261 (2011).
45. Ji, H. M. *et al.* Hybrid type-i inas/gaas and type-ii gasb/gaas quantum dot structure with enhanced photoluminescence. *Appl. Phys. Lett.* **106,** 103104 (2015).
46. Liao, Y.-A., Hsu, W.-T., Chiu, P.-C., Chyi, J.-I. & Chang, W.-H. Effects of thermal annealing on the emission properties of type-ii inas/gaassb quantum dots. *Appl. Phys. Lett.* **94,** 053101 (2009).
47. Sato, D. *et al.* Extremely long carrier lifetime at intermediate states in wall-inserted type ii quantum dot absorbers. *J. Appl. Phys.* **112,** 094305 (2012).
48. Pavarelli, N. *et al.* Competitive carrier interactions influencing the emission dynamics of gaassb-capped inas quantum dots. *Appl. Phys. Lett.* **101,** 231109 (2012).
49. Hodgson, P. D. *et al.* Blueshifts of the emission energy in type-ii quantum dot and quantum ring nanostructures. *Journal of Applied Physics* **114,** 073519 (2013).
50. Ledentsov, N. N. *et al.* Radiative states in type-ii gasb/gaas quantum-wells. *Phys. Rev. B* **52,** 14058–14066 (1995).
51. Kuokstis, E. *et al.* Two mechanisms of blueshift of edge emission in ingan-based epilayers and multiple quantum wells. *Appl. Phys. Lett.* **80,** 977–979 (2002).
52. Hatami, F. *et al.* Radiative recombination in type-ii gasb/gaas quantum dots. *Appl. Phys. Lett.* **67,** 656–658 (1995).
53. Landolt–Börnstein. *Numerical data and functional relationships in science and technology*, new series, Vol. III/17a (Springer, Berlin, 1982).
54. Llorens, J. M. *et al.* Type ii inas/gaassb quantum dots: Highly tunable exciton geometry and topology. *Appl. Phys. Lett.* **107,** 183101 (2015).

55. Reimer, M. E. *et al.* Overcoming power broadening of the quantum dot emission in a pure wurtzite nanowire. *Phys. Rev. B* **93,** 195316 (2016).
56. Turck, V. *et al.* Line broadening and localization mechanisms in cdse/znse quantum dots. *J. Lumin.* **87–9,** 337–340 (2000).
57. Grydlik, M. *et al.* Optical properties of individual site-controlled ge quantum dots. *Appl. Phys. Lett.* **106,** 251904 (2015).
58. Brokmann, X., Marshall, L. & Bawendi, M. Revealing single emitter spectral dynamics from intensity correlations in an ensemble fluorescence spectrum. *Opt. Express* **17,** 4509–4517 (2009).
59. Bakulin, A. A. *et al.* Charge trapping dynamics in pbs colloidal quantum dot photovoltaic devices. *Acs Nano* **7,** 8771–8779 (2013).

## Acknowledgements

The authors thank Alice Hospodková for her help with the sample preparation and Dominik Munzar, Dušan Hemzal, and Vlastimil Křápek for insightful discussions. A part of the work was carried out under the project CEITEC 2020 (LQ1601) with financial support from the Ministry of Education, Youth and Sports of the Czech Republic under the National Sustainability Programme II.

## Author Contributions

P.K. developed the CI code and the theory, interpreted the experimental data and wrote the manuscript. P.S. performed the measurements and provided figures with experimental data. D.G. provided the formal description of the CI theory presented in the supplement as well as performed the language correction of the manuscript.

## Additional Information

**Supplementary information** accompanies this paper at http://www.nature.com/srep

**Competing Interests:** The authors declare no competing financial interests.

**How to cite this article**: Klenovský, P. *et al.* Excitonic structure and pumping power dependent emission blue-shift of type-II quantum dots. *Sci. Rep.* **7**, 45568; doi: 10.1038/srep45568 (2017).

**Publisher's note:** Springer Nature remains neutral with regard to jurisdictional claims in published maps and institutional affiliations.